

Inverse focal shift: a new effect in truncated cylindrical waves

CARLOS J. ZAPATA-RODRÍGUEZ, MANUEL MARTÍNEZ-CORRAL, PEDRO ANDRÉS and AMPARO PONS

Department of Optics, University of Valencia, E-46100 Burjassot, Spain

(Received 2 April 1998; final revision received 16 July 1998)

Abstract. We report on a general analytical procedure to analyse the axial focusing properties of uniform cylindrical waves truncated by a rectangular window. The resulting on-axis diffraction pattern explicitly depends on the square of the window height-to-width ratio. Depending on the value of this parameter, different kinds of axial behaviour are observed. In particular, it is found that for low values of this parameter and low Fresnel number, instead of the expected focal-shift effect, an inverse focal-shift phenomenon can appear, i.e. the maximum of the axial-irradiance distribution is displaced further away from the window.

1. Introduction

The study of the focusing properties of spherical waves has been a subject of increasing interest over the last few decades [1–3]. Specifically, in the early 1980s it was analytically established [4–6], and experimentally verified [7] that when a monochromatic, uniform, converging spherical wave is diffracted by a circular aperture, in a low-Fresnel-number geometry, the maximum of the axial irradiance distribution is shifted toward the aperture. More recently it has been recognized that the focal-shift effect also appears in apodized systems [8–11] and an analytical formula has been reported for its evaluation [12].

This interesting effect has been found to appear also in other geometries, for example in truncated or nontruncated focused beams [13–17], in spherically aberrated focusing set-ups [18–20] and even in uniformly illuminated diffractive optical elements [21, 22].

In spite of this extensive analysis of the focal-shift phenomenon, not too much attention has been paid to the case of truncated cylindrical waves [19], which are of interest in, for example, optical signal processing [23, 24], line-focusing optics to produce a plasma sheet [25, 26], phase singularities generation in optical beams [27] and astigmatic laser mode inverters [28, 29], where anamorphic elements are extensively used.

In this paper, we develop an analytical formulation that fully describes the axial behaviour of cylindrical waves truncated by a rectangular window. Depending on the value of the here defined truncation ratio of the window, and considering a low-Fresnel-number focusing geometry, three different types of axial behaviour will be found. Specifically it will be shown that when the truncation in one Cartesian direction is neglected, a focal-shift effect appears, and an approximated

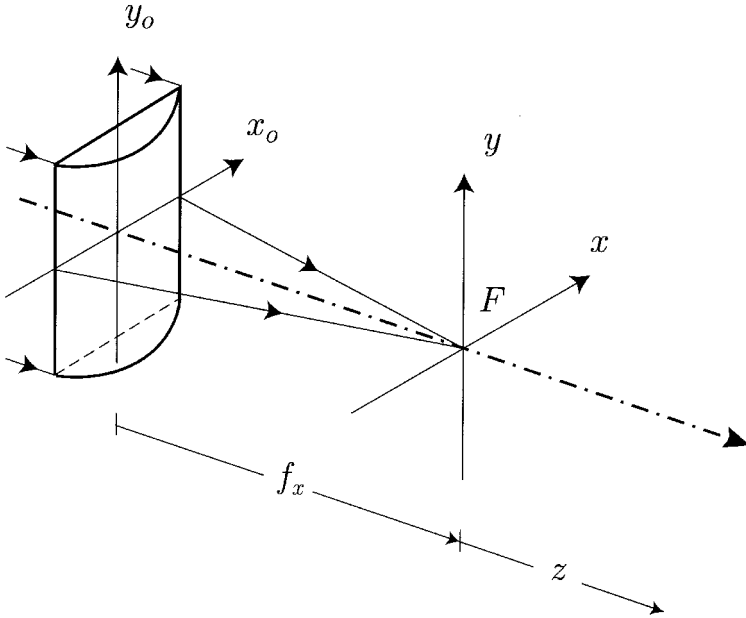


Figure 1. Schematic layout of the cylindrical focusing arrangement. The origin of the axial coordinate is taken at the focus F of the cylindrical lens.

formula for its evaluation is presented. On the contrary, when the truncation ratio is low, a new effect, the inverse focal shift, can appear. For intermediate values of the truncation ratio the axial-irradiance distribution has a steep-peaks structure in which the position of the maximum strongly depends on this parameter.

In Section 2 we formulate the basic theory for evaluating the axial-irradiance distribution for cylindrical waves. In Section 3 we generalize this analysis to the case of a two-dimensional (2D) rectangular truncation by giving an analytical formula that fully describes the corresponding axial behaviour. This formula will allow us to find that, under certain circumstances, an inverse focal-shift effect can appear. In Section 4 we carry out a thorough study of this new phenomenon, and some numerically evaluated examples are shown.

2. Axial-irradiance distribution

We start by considering a uniform, monochromatic plane wave of wavelength λ illuminating a cylindrical lens with a focal length denoted by f_x , as depicted in figure 1. Since the cylindrical lens produces over the emerging field a wave-front curvature along the x -axis, its amplitude transmittance can be expressed as

$$t(x, y) = p(x, y) \exp\left(-j\frac{k}{2f_x}x^2\right), \quad (1)$$

where $k = 2\pi/\lambda$ is the wave number, whereas the pupil function, $p(x, y)$, gives the window transmittance of the focusing element.

According to the Fresnel diffraction formula [30], the three-dimensional (3D) amplitude distribution in the focal region is given by

$$u(x, y, z) = A \frac{\exp[jk(z + f_x)]}{j\lambda(z + f_x)} \int_{-\infty}^{\infty} \int_{-\infty}^{\infty} t(x_0, y_0) \times \exp\left\{j \frac{k}{2(z + f_x)} [(x - x_0)^2 + (y - y_0)^2]\right\} dx_0 dy_0, \quad (2)$$

where A is a positive constant corresponding to the amplitude of the uniform illuminating field and z is the axial coordinate as measured from the geometrical focus, F , of the cylindrical lens.

To obtain the amplitude distribution along the optical axis, we substitute equation (1) into equation (2), then we set $x = y = 0$, giving

$$U(z) = A \frac{\exp[jk(z + f_x)]}{j\lambda(z + f_x)} \int_{-\infty}^{\infty} \int_{-\infty}^{\infty} p(x_0, y_0) \times \exp\left[-j \frac{k}{2f_x} \frac{z}{z + f_x} x_0^2\right] \exp\left[j \frac{k}{2(z + f_x)} y_0^2\right] dx_0 dy_0. \quad (3)$$

In the ideal case of an unapertured cylindrical lens, $p(x, y) = 1$, it is easy to find, by using the analytical relation

$$\int_{-\infty}^{\infty} \exp\left(j \frac{k}{2s} t^2\right) dt = (j\lambda s)^{1/2}, \quad (4)$$

that the axial-irradiance distribution is given by

$$I(z) = |U(z)|^2 = A^2 |f/z|. \quad (5)$$

Then, the maximum irradiance is located at the focus of the lens, $z = 0$, where a singularity caused by the unlimited extent of the 2D pupil function appears. Also, the dependence on the axial coordinate is inversely linear, which differs from the well-known inverse square law associated to uniform spherical waves. Therefore, the attenuation suffered by a cylindrical wave is weaker than that corresponding to a spherical field.

In a more realistic case, the finite extent of the cylindrical lens must be taken into account. Then we start by considering the case of a pupil aperture which is much higher along the y -axis, so that the truncation suffered by the field in this direction may be neglected. In this case we are allowed to carry out the substitution $p(x, y) = \text{rect}(x/a_x)$, where a_x denotes the extent of the slit-like pupil window. Therefore, according to equation (3) and by using again the relationship in equation (4), the axial-irradiance distribution can be written by

$$I(z) = A^2 \frac{1}{\lambda|z + f_x|} \left| \int_{-a_x/2}^{a_x/2} \exp\left[-j \frac{k}{2f_x} \frac{z}{z + f_x} x_0^2\right] dx_0 \right|^2. \quad (6)$$

As in conventional image formation formalism, it is convenient to express the out-of-focus behaviour of the focusing architecture in terms of the so-called defocus coefficient [31]. This coefficient is a small angle approximation ($a_x^2 \ll f_x^2$) for the distance between the wavefront created by the cylinder lens and a similar cylindrical wavefront with a curvature centred at the observation point P , taken at a point on the edge of the lens aperture along an axis normal to

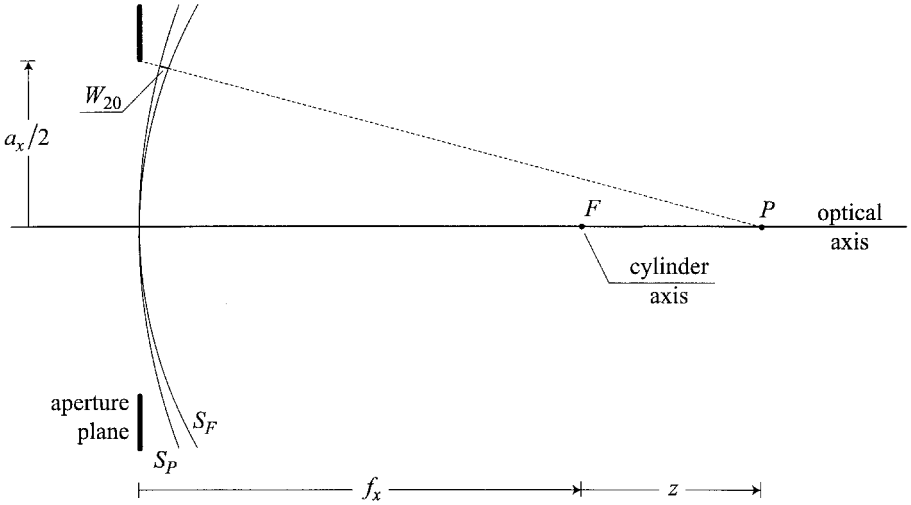


Figure 2. Schematic evaluation of the defocus coefficient W_{20} as the optical distance, attained at the edge of the lens window and expressed in units of the wavelength, between the cylindrical wavefront produced by the lens, S_F , and that whose focus is located at the axial point P .

the cylinder axis, and along the direction normal to the latter wavefront (see figure 2). In mathematical terms [32]

$$W_{20} = \frac{N_x}{2} \frac{z}{z + f_x}, \quad (7)$$

where

$$N_x = \frac{(a_x/2)^2}{\lambda f_x}, \quad (8)$$

stands for the so-called Fresnel number for the truncated, cylindrical focusing geometry, N_x . This parameter accounts for the number of cylindrical halfwave zones covered by the lens as viewed from its focus.

Then, by performing now an appropriate change of variables,

$$\xi = 2x_0/a_x, \quad (9)$$

and by normalizing to the value at the focus, the axial-irradiance distribution is determined by

$$\begin{aligned} I_N(W_{20}) &= \frac{I(W_{20})}{I(0)} = \left| 1 - \frac{2W_{20}}{N_x} \right| \left| \frac{1}{2} \int_{-1}^1 \exp(-j2\pi W_{20} \xi^2) d\xi \right|^2 \\ &\equiv \left| 1 - \frac{2W_{20}}{N_x} \right| |\psi(W_{20})|^2. \end{aligned} \quad (10)$$

In other words, the defocus coefficient W_{20} is $N_x/2$ times the ratio of the distance from the origin to the field point over the distance from the lens to the field point. Of course, it does not vary linearly as the field point moves away from the lens along the optical axis.

From equation (10) it is inferred that $I_N(W_{20})$ comprises the product of two terms. The first term describes the attenuation suffered by cylindrical waves as they propagate. This term is given by the function $|1 - 2W_{20}/N_x|$, which is centred at the axial coordinate $W_{20} = N_x/2$, which corresponds, of course, to the axial position $z = \infty$. The second term describes the diffraction effects due to the finite extent of the window in the x -direction, and is given by the squared modulus of the function $\psi(W_{20})$. This function may be analytically expressed by [33]

$$\psi(W_{20}) = \frac{1 - j \operatorname{erf}[(1 + j)(\pi W_{20})^{1/2}]}{4 \sqrt{W_{20}}}, \quad (11)$$

where $\operatorname{erf}[\bullet]$ is the error function, defined as

$$\operatorname{erf}[s] = \frac{2}{\sqrt{\pi}} \int_0^s \exp(-t^2) dt. \quad (12)$$

Although $|\psi(W_{20})|^2$ is an even function, the axial-irradiance distribution given by equation (10) is asymmetric in terms of z about the focal plane, $z = 0$, for two reasons. First, the defocus coefficient of equation (7) is asymmetric about the focal point, i.e. $|W_{20}(z)| \neq |W_{20}(-z)|$. Despite the asymmetric transformation suffered by this term, the maximum value of $|\psi(W_{20})|^2$ remains located at the origin. Second, the linear dependence on $|1 - 2W_{20}/N_x|$ increases the irradiance for $W_{20} < 0$, and so $z < 0$, within the focal region, and decreases it for $W_{20} > 0$. Therefore, the axial maximum appears shifted towards the pupil plane, resulting in the so-called focal shift effect for cylindrical waves, as described in reference [19].

However, W_{20} is antisymmetric about $z = 0$, i.e. $W_{20}(-z) = -W_{20}(z)$, for very small z where it is approximately given by $W_{20} \approx N_x z / 2f_x$. Now, for very large N_x the depth of focus given by the second term in equation (10) is small so that for the small range of z within the focal spot, W_{20} is antisymmetrical. In this case, the term $|1 - 2W_{20}/N_x|$ tends to unity, so that the irradiance pattern is symmetric about the geometrical focus, and the maximum irradiance is located at the origin. As soon as the Fresnel number decreases the depth of focus is very large so that the asymmetry in W_{20} yields the axial-irradiance distribution asymmetric, and the asymmetry in the linear term shifts the peak of the focal spot towards the lens.

To illustrate this effect, we have depicted in figure 3 the normalized axial-irradiance distribution for difference values of N_x . It is apparent from this figure that the lower is the value of N_x , the greater is the attained focal shift.

As in the case of a spherically illuminated circular aperture [4], now we can find a simple formula that accurately evaluates the amount of focal shift for moderate values of N_x . For that purpose we expand the axial-irradiance distribution into a Taylor series up to a second order approximation, that is

$$I_N(W_{20}) \approx I_N(0) + I'_N(0)W_{20} + \frac{1}{2}I''_N(0)W_{20}^2 = 1 - \frac{2}{N_x}W_{20} - \frac{16\pi^2}{45}W_{20}^2, \quad (13)$$

where $I'_N(\bullet)$ and $I''_N(\bullet)$ denote the first- and second-order derivative of the function $I_N(W_{20})$, respectively. By taking the derivative of equation (13), and by setting it equal to zero, we find that the irradiance distribution is not symmetrical with respect to the focal point, $W_{20} = 0$, but to the shifted point of axial coordinate

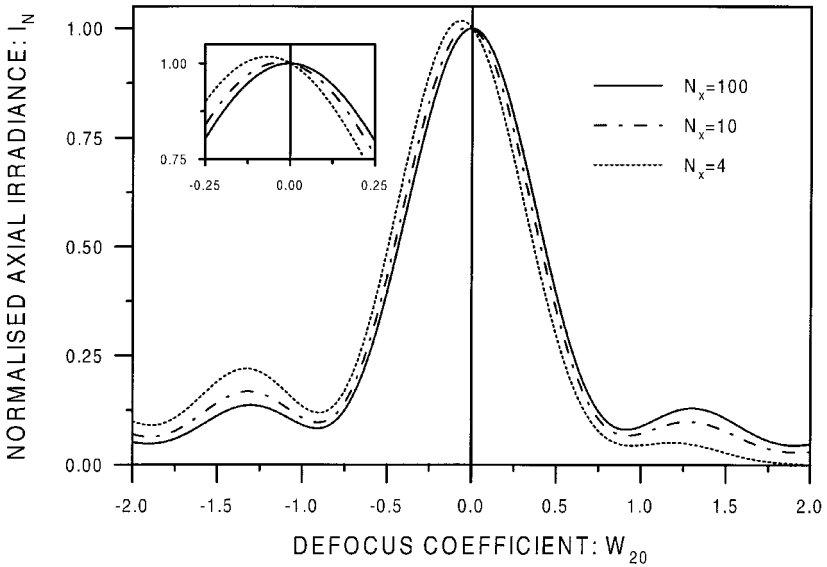


Figure 3. Axial-irradiance distribution corresponding to a slit-like window from equation (10). The on-axis behaviour is shown for three values of the Fresnel number: $N_x = 100$ (high), $N_x = 10$ (moderate), $N_x = 4$ (low).

$$W_{20}^{\max} = -\frac{45}{16\pi^2 N_x}, \quad (14)$$

where the maximum axial irradiance is attained. It seems more appropriate to express the focal shift in terms of the spatial axial coordinate, z . Hence, by combining equations (7) and (14) we find that the relative axial position of the irradiance maximum, that is, the relative focal shift, is expressed as

$$\frac{z_{\max}}{f_x} = -\frac{1}{1 + \frac{8\pi^2}{45} N_x^2}. \quad (15)$$

The minus sign in equation (15) indicates that, either in the case of a converging ($f_x > 0$) or a diverging ($f_x < 0$) cylindrical lens, the displacement of the axial-irradiance peak is always directed toward the lens. It is also remarkable that this equation is of the same form as the expression corresponding to the exact relative focal shift in a focused cylindrical Gaussian beam of Gaussian Fresnel number $N_G^2 = 8N_x^2/45$ [13]. Note that although in reference [13] the case of spherical Gaussian beams is analysed, it is easy to show that the focal shift for spherical and cylindrical Gaussian beams, both with the same waist, are equal.

To illustrate the accuracy of equation (15), in figure 4 we have represented the value of the relative focal shift obtained with the approximated formula, and its exact value derived from equation (10). The examination of this figure reveals that the approximated formula gives suitable results for moderate and high values of N_x (for example, when $N_x = 5$ the error is 2.2% and for $N_x = 50$ the error is less than 0.6%).

Finally, we would like to point out that although this analysis is equivalent to that performed by Jiang and Stammes [19], our approach shows considerable

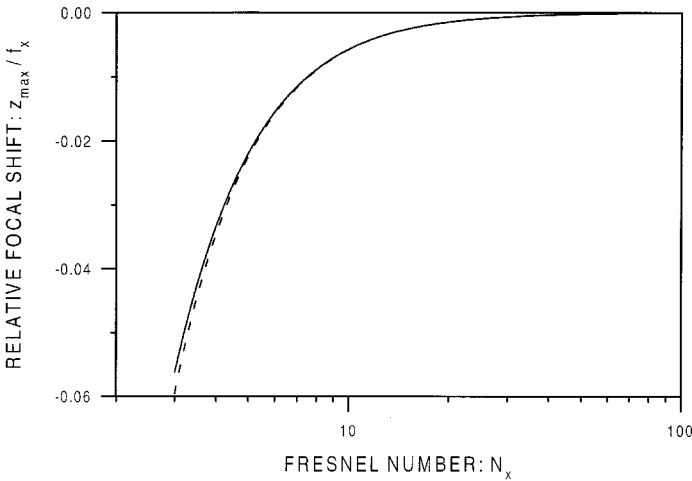


Figure 4. Relative focal shift versus Fresnel number N_x evaluated by means of equation (15) (dashed line) and by exact numerical calculations from equation (10) (solid line).

improvements. On the one hand, the results have been generalized to the case of diverging cylindrical waves. On the other hand, an approximated formula, which accurately evaluates the amount of focal shift for moderate values of N_x , is obtained [see equation (15)].

The analysis carried out above is appropriate for a great part of the practical cases found in the laboratory, in which the pupil aperture is much higher along the y -direction. Nevertheless, it seems that the assumption of infinity extent of the focusing element along the y -direction is quite stringent. Therefore it is necessary to perform a more general treatment of the problem, as will be done in the next section.

3. The case of a 2D rectangular window

In order to take into account the finite extent of the exit pupil in the two Cartesian directions, we assume a rectangular window function $p(x, y) = \text{rect}(x/a_x) \text{rect}(y/a_y)$. By substituting this pupil function into equation (3) and by performing the changes of variable

$$\xi = \frac{2x_0}{a_x}, \quad \xi = \frac{2y_0}{a_y}, \quad (16)$$

it is straightforward to find that

$$\begin{aligned} I(W_{20}) &= A^2 N_x^2 T^2 \left(1 - \frac{2W_{20}}{N_x}\right)^2 \left| \int_{-1}^1 \exp(-j2\pi W_{20} \xi^2) d\xi \right|^2 \\ &\quad \times \left| \int_{-1}^1 \exp[-j2\pi T(W_{20} - N_x/2)\xi^2] d\xi \right|^2, \end{aligned} \quad (17)$$

where we have introduced a new parameter, named here the truncation ratio, defined as $T = (a_y/a_x)^2$.

The normalized axial-irradiance distribution may be expressed by

$$I_N(W_{20}) = \chi(W_{20})|\psi(W_{20})|^2, \quad (18)$$

where

$$\chi(W_{20}) = \frac{1}{|\psi(-N_x T/2)|^2} \left(1 - \frac{2W_{20}}{N_x}\right)^2 \left|\psi\left(\frac{W_{20} - N_x/2}{1/T}\right)\right|^2. \quad (19)$$

This relevant formula, that fully describes the axial behaviour of cylindrical lenses for any value of N_x and any truncation ratio, indicates that the axial-irradiance distribution is governed by the product of two different factors. The first factor, $|\psi(W_{20})|^2$, has already been described in Section 2. Regarding the second term, $\chi(W_{20})$, it is an even function centred at $W_{20} = N_x/2$, and describes both the diffraction effects due to the finite extent of the pupil along the y -direction, which explicitly depends on the value of T , and the irradiance attenuation inherent to wave propagation.

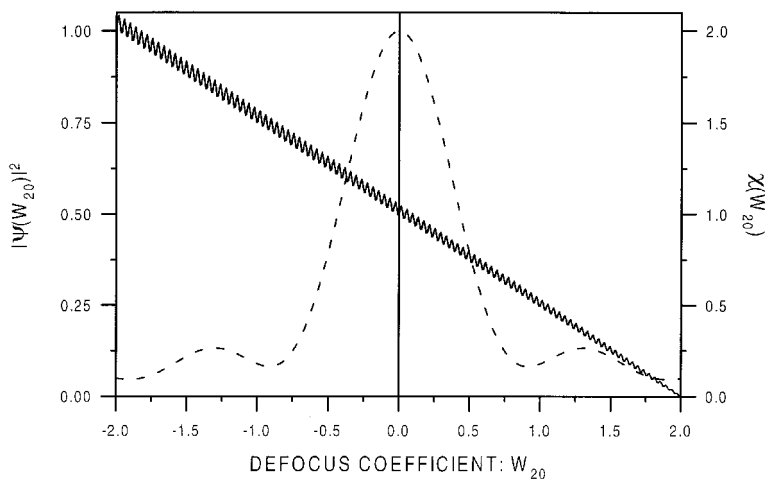
Now, we can give some general remarks on the axial behaviour of cylindrical lenses by examining its dependence with the parameter T . For this task, we assume a fixed value of the Fresnel number of the focusing geometry, say $N_x = 4$. First, we investigate the case in which the truncation parameter is much higher than unity. In this case, the function $\chi(W_{20})$ tends to $\chi(W_{20}) = |1 - 2W_{20}/N_x|$. Therefore, the axial behaviour is similar, of course, to that of cylindrical fields nontruncated along the y -direction, which indeed was described by equation (10).

When the value of the truncation ratio decreases, the function $\chi(W_{20})$ exhibits a high-frequency sinusoidal-like variation modulating a dominant linear dependence. In fact, the frequency of the modulation is proportional to the value of T , as is illustrated in figure 5, where we have represented the function $\chi(W_{20})$ for two different values of T .[†] When the product of the two terms, $\chi(W_{20})$ and $|\psi(W_{20})|^2$, is performed, an axial-irradiance distribution is obtained in which a rapidly varying ripple structure is dominant on the total profile, as is shown in figure 6. Note from this figure that the central lobe has a steep-peaks structure in which the position of the maximum strongly depends on the value of T .

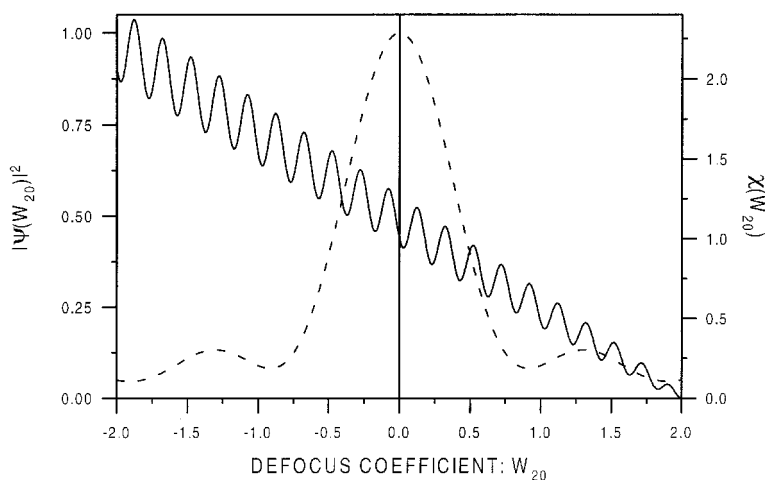
When the truncation ratio is lower than unity, for example $T = 0.33$, the function $\chi(W_{20})$ has a slowly-varying behaviour so that the slope in the vicinities of the geometrical focus is positive, in opposition to the negative slope corresponding to very high values of T . When this function is multiplied by the term $|\psi(W_{20})|^2$, which is an even function with maximum value at the origin, an axial pattern is obtained in which the irradiance peak is now moved further from the lens, as shown in figure 7(b).

The appearance of this new phenomenon, which we will refer to as the inverse focal-shift effect, seems to be mainly determined by the scale of $\chi(W_{20})$ and its slope at the origin. In the next section we carry out a thorough analysis of this effect in order to find out when a cylindrical focusing geometry tends to suffer inverse focal shift.

[†] The calculation of the data for most of the curves in this paper involves the evaluation of the function $\text{erf}[\bullet]$. This function is included in standard mathematical packages, for example Matlab or Mathematica. In particular, our calculations were performed using Mathematica.



(a)



(b)

Figure 5. Graphical representation of the functions $|\psi(W_{20})|^2$ (dashed curve) and $\chi(W_{20})$ (solid curve) in a low-Fresnel-number system, $N_x = 4$. The truncation ratios are: (a) $T = 100$, (b) $T = 10$.

4. The inverse focal shift

The study of figures shown in section 3 reveals that for the appearance of an inverse focal-shift effect a twofold condition must be satisfied. On the one hand, the frequency of the ripples structure of function $\chi(W_{20})$ must be low enough so that less than one ripple lies in the core region of $|\psi(W_{20})|^2$. Therefore, the value of T must be lower than unity. On the other hand, the slope of $\chi(W_{20})$ in the vicinities of the geometrical focus, $W_{20} = 0$, must be positive.

The analysis of equation (19) indicates that (a) the scale of curve $\chi(W_{20})$ is inversely proportional to T , (b) the curve is centred at $W_{20} = N_x/2$, and (c) independently of the particular values of the parameters N_x and T , the part of the curve that is in the geometrical focus is determined by the value of the product

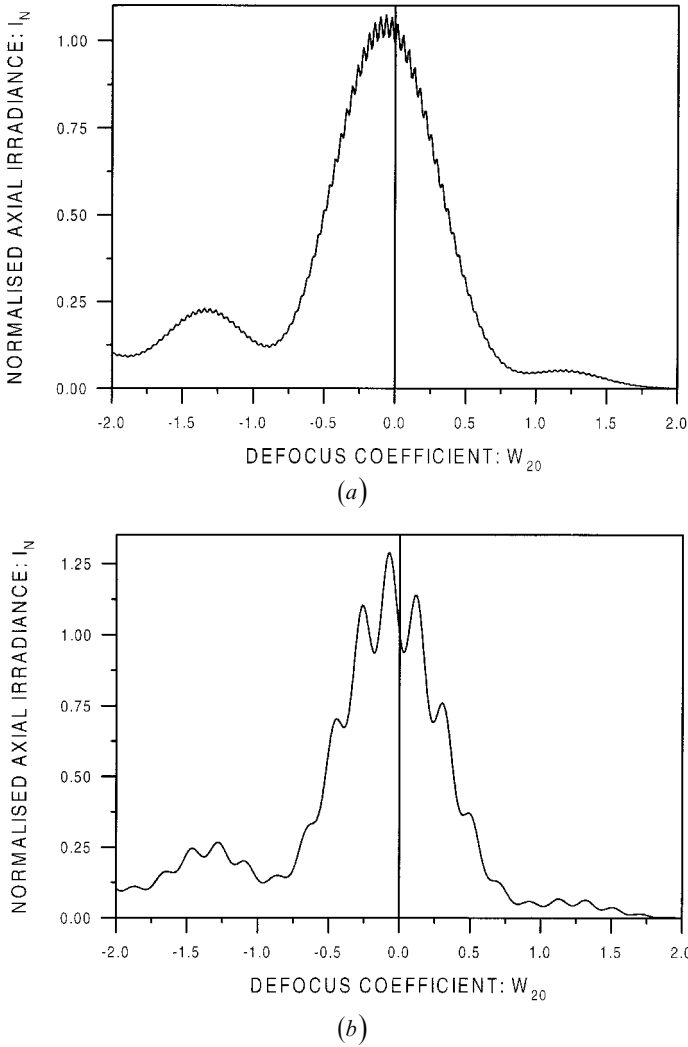
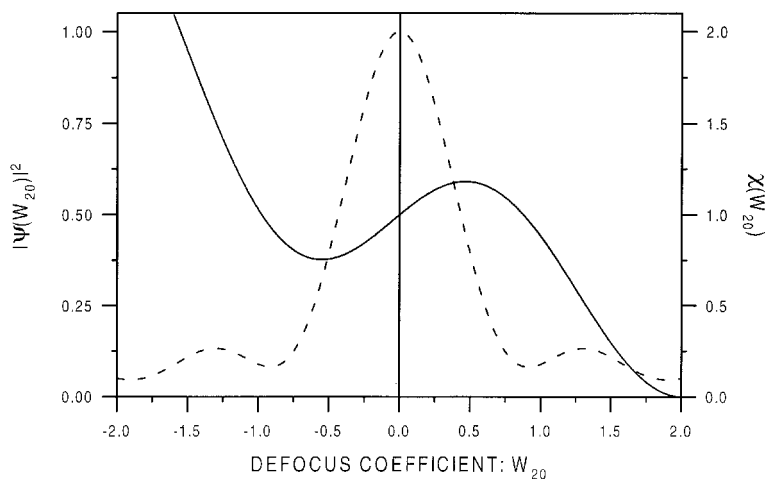


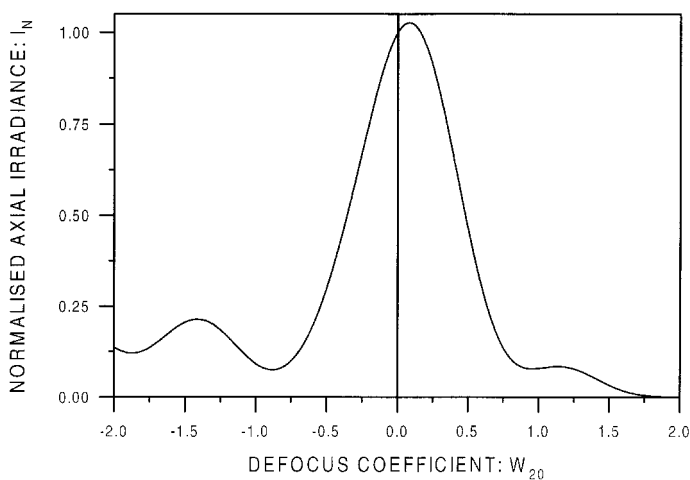
Figure 6. Axial-irradiance distribution obtained according to equation (18) by the product of the terms $|\psi(W_{20})|^2$ and $\chi(W_{20})$. We have selected the values of the Fresnel number and the truncation ratio from figure 5.

$N_x T$. Note then that, under the constraint $N_x T = \text{constant}$, a change in the value of N_x results in a displacement of the $\chi(W_{20})$ curve. However, this displacement is accompanied by a proportional change of the scale so that the same ripple of the curve always remains in the vicinity of the focus. To illustrate this property, in figure 8 we have plotted the curve $\chi(W_{20})$ for three different arrangements with $N_x T = \text{constant}$.

From the above reasoning it is then apparent that an inverse focal-shift effect similar to that shown in figure 8 can be obtained with other cylindrical focusing geometries, provided that the product $N_x T$ remains constant. Note, however, that under this constraint, the lower is the value of N_x , the higher is the slope of $\chi(W_{20})$ and, consequently, the higher is the amount of the resulting inverse focal shift (see



(a)



(b)

Figure 7. Graphical analysis of the cylindrical focusing set-up characterized by a Fresnel number $N_x = 4$ and a truncation ratio $T = 0.33$ by representing: (a) the functions $|\psi(W_{20})|^2$ and $\chi(W_{20})$, and (b) the normalized axial-irradiance distribution from equation (18).

figure 9). However, if N_x is too low, and then T too high, an axial pattern with a rapidly varying ripples structure results again.

A result is then obtained that is, in a certain way, similar to that corresponding to a spherically illuminated circular aperture, in which the lower the Fresnel number of the focusing set-up, the higher the magnitude of the focal shift.

To mathematically support the above heuristic reasoning, next we calculate the ratio, evaluated at the origin, between the first derivative of $\chi(W_{20})$ corresponding to any two different arrangements characterised by $N_{x,1}T_1 = N_{x,2}T_2$. The ratio is in the form

$$\frac{\chi_1'(0)}{\chi_2'(0)} = \frac{T_1}{T_2} = \frac{N_{x,2}}{N_{x,1}}. \quad (20)$$

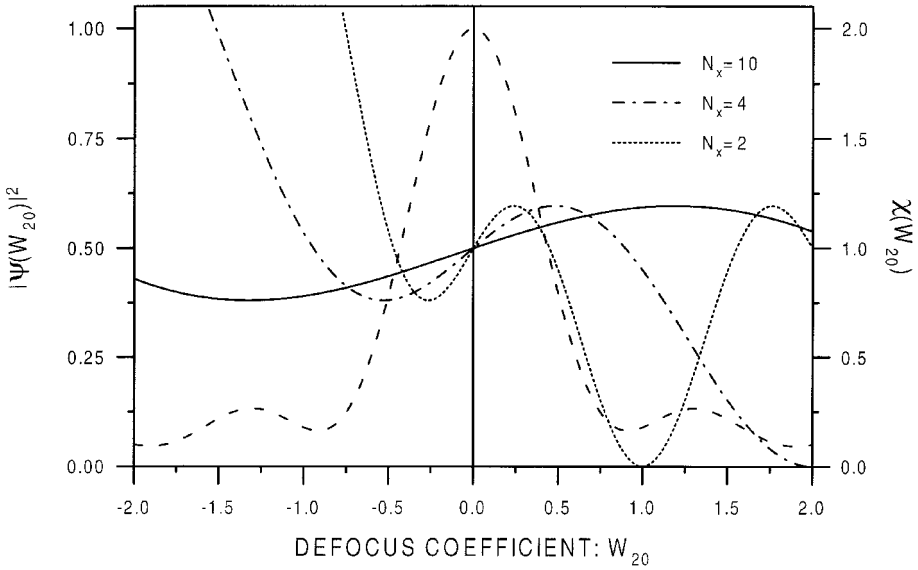


Figure 8. Variation of $\chi(W_{20})$ for three different arrangements imposing $N_x T = 1.33$.

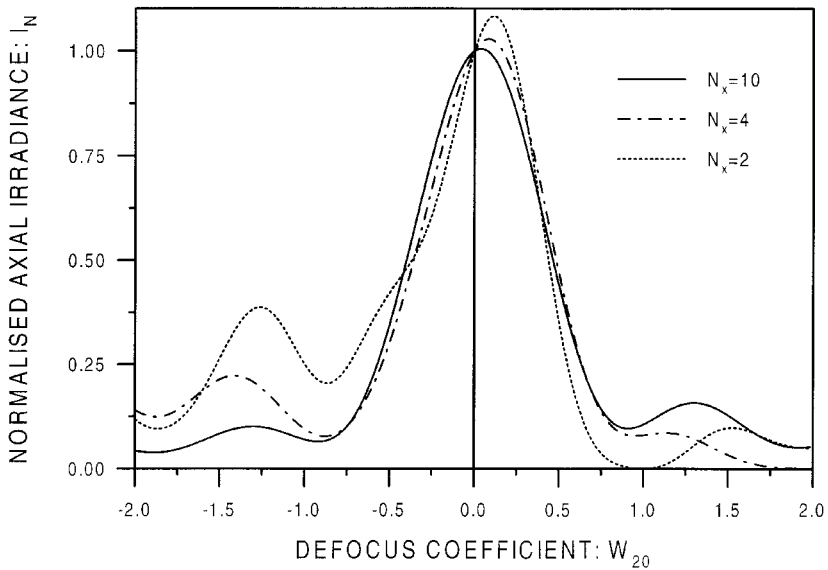


Figure 9. Normalized axial pattern I_N of the cylindrical focusing geometries analysed in figure 8.

This equation confirms that, if $N_x T = \text{constant}$, the slope of $\chi(W_{20})$ at the origin is inversely proportional to N_x . Moreover, the sign of the slope remains unaltered.

Up to now, we have centred our analysis on the inverse focal shift that appears when the positive slope of the first ripple of $\chi(W_{20})$ lies in the focal region. However, it is clear that a similar effect appears when the positive slope of a further ripple lies in the vicinity of the focus. To analyse this property, we have numerically evaluated equation (19) in order to find out which values of the

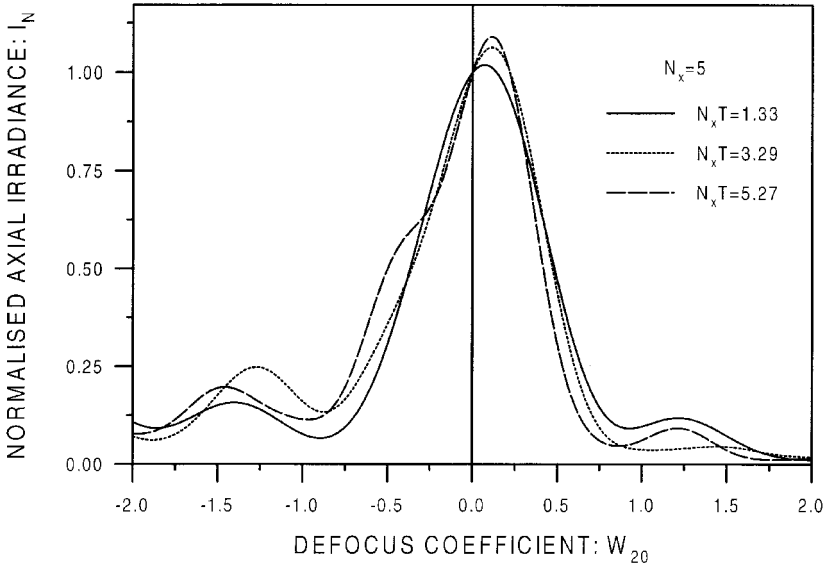


Figure 10. Normalized axial-irradiance distribution for three different focusing arrangements where the positive slopes for the first, second and third ripple of the function $\chi(W_{20})$ lie in the focal region.

Table 1. Values of the product $N_x T$ giving rise to a relative extreme of the function $\chi(W_{20})$ at the origin, $W_{20} = 0$.

Order of the ripple	$(N_x T)_{\max}^i$	$(N_x T)_{\min}^i$
$i = 1$	1.01	1.68
$i = 2$	2.88	3.69
$i = 3$	4.84	5.70
$i = 4$	6.83	7.71
$i = 5$	8.82	9.71
\vdots	\vdots	\vdots
$i = n + 1$	$(N_x T)_{\max}^n + 2$	$(N_x T)_{\min}^n + 2$

product $N_x T$ give rise to a positive slope of $\chi(W_{20})$ in the focal point. In table 1 we have listed the values of $N_x T$ which provide a maximum or a minimum at $W_{20} = 0$.

Based on the materials in this table, we may establish the following properties: cylindrical focusing set-ups with $N_x T$ lying in an interval $[(N_x T)_{\max}^i, (N_x T)_{\min}^i]$, suffer from an inverse focal shift (see figure 10). Moreover, the inverse focal shift is much higher when the value of $N_x T$ is in the centre of the interval, whereas it vanishes when $N_x T$ is close to one of the extremes.

Another interesting effect takes place when the value of $N_x T$ lies in an interval $[(N_x T)_{\min}^i, (N_x T)_{\max}^{i+1}]$, which corresponds to a case in which the slope of $\chi(W_{20})$ in the focal region is negative. In this case the product between $\chi(W_{20})$ and $|\psi(W_{20})|^2$ provides an axial-irradiance distribution in which the maximum is shifted toward the lens. Thus, it results in a conventional focal shift effect (see figure 11). It is worthy to remark that also in this case a slight change in the value of $N_x T$ implies a

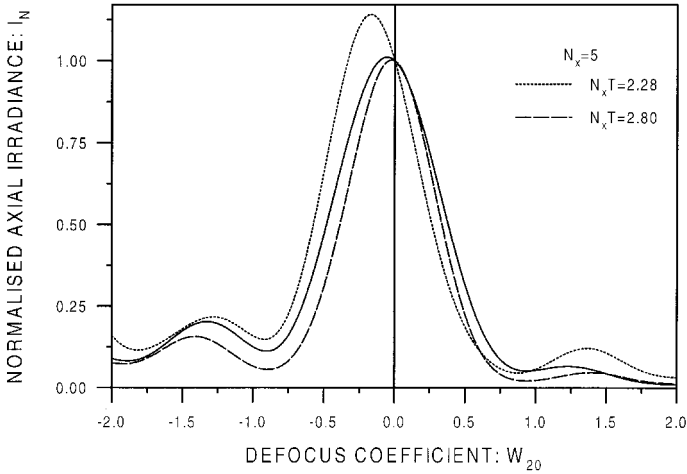


Figure 11. Axial-irradiance distribution I_N corresponding to two values of $N_x T$ giving rise to a negative slope of the function $\chi(W_{20})$ in the focal region. Both plots are compared with that of a nontruncated cylindrical wave along the y -direction (solid line), which results in the conventional focal shift phenomenon. We observe an enhanced ($N_x T = 2.28$) and attenuated ($N_x T = 2.80$) focal-shift effect.

change in the slope of $\chi(W_{20})$ and then a variation in the magnitude of the focal shift.

From the above results we conclude that one can gradually modify the magnitude of the focal shift by continuously varying the value of $N_x T$. This variation from a practical point of view can be implemented, e.g. by getting fixed N_x and varying the width of the window along the y -direction. In this way, one can alternatively obtain, for example an enhanced focal shift, an attenuated focal shift or an inverse focal shift of variable magnitude.

5. Conclusions

We have derived an analytical formulation for evaluating the on-axis diffraction behaviour of uniform cylindrical waves truncated by a rectangular window. It has been shown that the resulting axial pattern is governed by two parameters: the Fresnel number of the cylindrical focusing geometry, N_x , and the here defined truncation ratio of the window, T . For very high values of T , it is shown that, depending on the value of N_x , a focal-shift effect can appear. Moreover, an approximated formula, which accurately evaluates the amount of focal shift for moderate values of N_x , is obtained.

The most important outcome of this research is the achievement and subsequent analysis of an inverse focal-shift effect. In particular, it has been found that this phenomenon appears in principle when the value of the product $N_x T$ is low (about 1.33). However, we have shown that this effect also appears for higher values of $N_x T$, provided that a slowly varying increasing slope of the function $\chi(W_{20})$ lies in the focal region.

Contrary to what happens in the case of the conventional focal shift phenomenon, it does not seem possible to obtain a simple analytical formula to evaluate the

amount of inverse focal shift. This is because in this case the number of parameters involved is much higher.

In order to find the physical significance of the product $N_x T$, we can decompose the axial-irradiance distribution in equation (18) into two different terms. The first one, which coincides with that given in equation (10), corresponds to the on-axis pattern of a uniform cylindrical wave diffracted by an unlimited slit along the meridian with no power and, as shown in Section 2, in this case the axial behaviour depends on the Fresnel number N_x . The second factor, $|1 - 2W_{20}/N_x| |\psi[(W_{20} - N_x/2)/(1/T)]|^2$, represents the irradiance distribution along the optical axis obtained for a uniform plane wave diffracted by a slit aperture of height a_y [34]. Moreover, in agreement with equation (8) we can rewrite the parameter $N_x T$ as $N_x T = (a_y/2)^2/\lambda f_x$. In this context, this quantity provides the number of cylindrical Fresnel zones that will be visible from an axial point located at a distance f_x . The resulting nonmonotonic axial behaviour then produces, for certain values of this new Fresnel number, $N_x T$, a negative slope at $W_{20} = 0$ which features the inverse focal shift.

Finally, we have shown that by simply modifying the value of $N_x T$ one can gradually tune the magnitude of the inverse focal-shift effect, even to obtain a variable focal-shift phenomenon. To illustrate our result, some numerically evaluated examples have been presented.

We would like to conclude by emphasizing that although no experimental results have been presented in this paper, we consider that it cannot be hard to measure the inverse focal shift if, for example, a technique similar to that proposed by Karman *et al.* is used [35, 36].

Acknowledgments

This work was supported by the Dirección General de Investigación Científica y Enseñanza Superior (grant PB93-0354-C02-01), Ministerio de Educación y Ciencia, Spain. C. J. Zapata-Rodríguez gratefully acknowledges financial support from this institution.

References

- [1] COLLET, E., and WOLF, E., 1980, *Optics Lett.*, **5**, 264.
- [2] BORN, M., and WOLF, E., 1980, *Principles of Optics*, 6th edn, (Oxford: Pergamon), Sec. 8.8.1.
- [3] WANG, W., and WOLF, E., 1995, *Optics Commun.*, **119**, 453.
- [4] LI, Y., and WOLF, E., 1981, *Optics Commun.*, **39**, 211.
- [5] STAMNES, J. J., and SPEJLKAVIK, B., 1981, *Optics Commun.*, **40**, 81.
- [6] MAHAJAN, V. N., 1983, *Appl. Optics*, **22**, 3042.
- [7] LI, Y., and PLATZER, H., 1983, *Optica Acta*, **30**, 1621.
- [8] OJEDA-CASTAÑEDA, J., MARTÍNEZ-CORRAL, M., ANDRÉS, P., and PONS, A., 1994, *Appl. Optics*, **33**, 7616.
- [9] SZAPIEL, S., 1983, *Optics Lett.*, **8**, 327.
- [10] MARTÍNEZ-CORRAL, M., ANDRÉS, P., and OJEDA-CASTAÑEDA, J., 1994, *Appl. Optics*, **33**, 2223.
- [11] MARTÍNEZ-CORRAL, M., and CLIMENT, V., 1996, *Appl. Optics*, **35**, 24.
- [12] MARTÍNEZ-CORRAL, M., ZAPATA-RODRÍGUEZ, C. J., ANDRÉS, P., and KOWALCZYK, M., 1998, *J. mod. Optics*, **45**, 1671.
- [13] CARTER, W. H., 1982, *Appl. Optics*, **21**, 1989.

- [14] LI, Y., and WOLF, E., 1982, *Optics Commun.*, **40**, 151.
- [15] LI, Y., 1992, *J. mod. Optics*, **39**, 1761.
- [16] MARTÍNEZ-CORRAL, M., ZAPATA-RODRÍGUEZ, C. J., ANDRÉS, P., and SILVESTRE, E., 1998, *J. opt. Soc. Am. A*, **15**, 449.
- [17] PU, J., 1998, *J. mod. Optics*, **45**, 239.
- [18] YOSHIDA, A., and ASAKURA, T., 1994, *Optics Commun.*, **119**, 368.
- [19] JIANG, D. Y., and STAMNES, J., 1997, *Pure Appl. Optics*, **6**, 85.
- [20] FURLAN, W. D., SAAVEDRA, G., SILVESTRE, E., and MARTÍNEZ-CORRAL, M., 1998, *J. mod. Optics*, **45**, 69.
- [21] HESSLER, T., and KUNZ, R. E., 1997, *J. opt. Soc. Am. A*, **14**, 1599.
- [22] LI, Y., 1997, *J. opt. Soc. Am. A*, **14**, 1297.
- [23] GRANIERI, S., FURLAN, W. D., SAAVEDRA, G., and ANDRÉS, P., 1997, *Appl. Optics*, **36**, 8363.
- [24] MENDLOVIC, D., BITRAN, Y., DORSCH, R. G., FERREIRA, C., GARCIA, J., and ÖZAKTAZ, H. M., 1995, *Appl. Optics*, **34**, 7451.
- [25] YOON, G.-Y., JITSUNO, T., KATO, Y., and NAKATSUKA, N., 1997, *Appl. Optics*, **36**, 847.
- [26] SHEN, W., SCHARER, J. E., LAM, N. T., PORTER, B. G., and KELLY, K. L., 1995, *J. appl. Phys.*, **78**, 6974.
- [27] PETROV, D. V., CANAL, F., and TORNER, L., 1997, *Optics Commun.*, **143**, 265.
- [28] NIENHUIS, G., 1996, *Optics Commun.*, **132**, 8.
- [29] COURTIAL, J., DHOLAKIA, K., ALLEN, L., and PADGETT, M. J., 1997, *Optics Commun.*, **144**, 210.
- [30] GOODMAN, J. W., 1968, *Introduction to Fourier Optics* (New York: McGraw-Hill), Chap. 4.
- [31] HOPKINS, H. H., 1950, *Wave Theory of Aberrations* (Oxford: Clarendon), p. 11.
- [32] STOKSETH, A., 1969, *J. opt. Soc. Am.*, **59**, 1314.
- [33] ABRAMOWITZ, M., and STEGUN, I. A., 1972, *Handbook of Mathematical Functions* (New York: Dover), p. 297.
- [34] SIEGMAN, A. E., 1986, *Lasers* (Mill Valley: University Science Books), Chap. 18.
- [35] SUCHA, G. D., and CARTER, W. H., 1984, *Appl. Optics*, **23**, 4345.
- [36] KARMAN, G. P., VANDUIJL, A., BEIJERSBERGEN, M. W., and WÖERDMAN, J. P., 1997, *Appl. Optics*, **36**, 8091.